ICAS Paper No. 70-49

THE EXTERNAL DRAG AT SUBSONIC AND SUPERSONIC SPEEDS OF FUSELAGE-SIDE INTAKES FOR STRIKE-FIGHTER AIRCRAFT

by
M. D. Dobson, Senior Scientific Officer
and
E. L. Goldsmith, Principal Scientific Officer
Royal Aircraft Establishment
Bedford, U.K.

The Seventh Congress of the International Council of the Aeronautical Sciences

CONSIGLIO NAZIONALE DELLE RICERCHE, ROMA, ITALY / SEPTEMBER 14-18, 1970

Price: 400 Lire

THE EXTERNAL DRAG AT SUBSONIC AND SUPERSONIC SPEEDS OF FUSELAGE-SIDE AIR INTAKES FOR STRIKE-FIGHTER AIRCRAFT

M. D. Dobson and E. L. Goldsmith

Royal Aircraft Establishment

Bedford, England

Abstract

Experiments designed to measure the external drag of fuselage-side intakes are described. The drag associated with varying internal flows has been measured and the effects on drag of changes of intake design (e.g. cowl lip radius, compression surface angle or position etc.) have been measured and compared with estimates.

Introduction

Multi-mission combat aircraft, as their name implies, have to perform efficiently over a wide range of flight speed, engine speed and aircraft attitude. They must be able to operate at sea level at high subsonic or low supersonic speeds to evade detection, to climb to high altitude for interception purposes at Mach numbers from 2.0 to 2.5 and to cruise at high altitude at M_∞ = 0.6 to 0.8 to achieve long range.

Most of these aircraft designs feature twin engines mounted in the fuselage and fed by air from intakes on the sides of the fuselage, exhausting via twin nozzles at, or upstream of the end of the fuselage. As is well known, the correct representation of intake flow and nozzle exhaust flow, and the simultaneous measurement of external forces poses one of the major problems in wind tunnel testing. Often the only way to obtain accurate measurements (particularly of drag) is to study the effects of intake or exhaust flow representation on partial models that do not fully represent the complete aircraft. Results from these tests then have to be related to tests on complete aircraft models where probably the intake and exhaust flows have not been simulated correctly.

The subject of this paper is an account of tests made with one particular partial model which measures the drag at subsonic and supersonic speeds of twin intakes on the sides of a fuselage. The technique of mounting the fuselage plus intakes on a balance, 'earthing' the intake flow control valves and measuring internal and base drags to obtain external drag is similar to that used by NASA during the middle and late 1950s.

In the design of fuselage, sting, intakes, flow control and means of pressure measurement emphasis has been placed on:-

(a) obtaining versatility in the arrangement that can be tested, i.e. type of intake, its position relative to the fuselage and its detail geometry (cowl and compression surface shapes etc.).

(b) ensuring that the necessary accuracy can be obtained for required components of external drag, e.g. spillage, diverter or cowl drag etc.

In the analysis of results emphasis is placed on comparison of measured results with predicted values. Where this can be done with some precision (e.g. change in pre-entry drag at full flow for semi-circular intakes at supersonic speeds), if comparison is satisfactory, confidence is gained in the general accuracy of the experiment.

Calculations of the drag of aircraft at transonic and supersonic speeds are usually made using one of the various forms of area rule in which there are inherent assumptions of low surface slope and attached shock waves. The intake is assumed to be operating at full flow and the stream tube corresponding to this condition is subtracted from the area distribution of the aircraft. The measurements in this paper are concerned with the real flow associated with practical installed intakes which includes for example, detached shock waves resulting from high initial cowl slopes and compression surface inclinations, subsonic fore-spillage due to variation in engine flow requirements and the presence of a wedge shaped boundary layer diverter. The drag associated with these is investigated and in some cases comparison is made with theoretical estimates.

Experimental details

The wind tunnel model consists of a forward fuselage constructed in the form of a fork, Fig.1(a) in which the two prongs form dorsal and ventral spines along the length of the model. A nose and canopy fit onto this fork and the whole is supported on a sting which incorporates a five component strain gauge balance, Fig.1(b). Sides carrying the intake nacelles secured between the spines of the fuselage complete the model, Fig.1(c). With this arrangement various intake designs, typical of this type of installation, may be tested, all utilising the same basic rig. For a given type of intake, detail design changes are effected by making cowls, compression surfaces etc. interchangeable. There is also facility for varying the design and position of the means used to divert or duct away the fuselage boundary layer. Hitherto simple wedge diverters have been used and their depth h_D (see Fig.3) is varied by adjusting the entire nacelle laterally with respect to the fuselage, by sliding it between the parallel surfaces of the fuselage spines. The fuselage sides have been made flat, Fig.2(a), so that the diverter depth is constant over the span of the intake. The intakes (nacelles) may be removed and replaced by flat sides, Fig.2(b), to give a 'clean' fuselage configuration.

Three components of drag are measured which are combined to give the total external drag coefficient of the model C_{D_E}, as

$$C_{D_E} = \frac{D_E}{q_\infty 2A_e} = C_{D\ BAL} - C_{D\ BASE} - C_{DI}$$

in which:-

$C_{D\ BAL}$ = drag coefficient measured by the balance

$C_{D\ BASE}$ = base drag coefficient

C_{DI} = sum of the measured internal drag coefficients of the two ducts.

Base drag is measured using an array of fifteen forward facing pressure tubes, three of which are shown in Fig.2(c). These tubes are secured to the sting and positioned close to the model base. Distribution of base pressure has been examined for various test conditions and individual pressure tubes are located to give increased coverage in regions where pressure gradients occur. The pressure measured by each tube is area weighted accordingly in the calculation of base drag. The periphery of the base of the model and the duct exits have been shrouded, Fig.2(c), in an attempt to improve the uniformity of base pressure.

The internal flow is controlled and measured by instrumentation which is 'earthed' to the sting support and therefore the drag associated with it does not appear in the internal drag calculation. The equation used in the calculation of internal drag is:-

$$C_{DI} = \frac{2A_\infty}{A_e} - \frac{1}{q_\infty}\frac{A_x}{A_e}\left[(p_x - p_\infty) + \gamma p_x M_x^2\right]$$

which gives the internal drag from a free stream station to the measuring station in the model duct. The internal instrumentation does not measure the skin friction drag on the parallel duct wall between the measuring station and the exit. This quantity is calculated using flat plate skin friction data[1].

To ensure sufficient accuracy in the measurement of internal mass flow, the model ducts and instrumentation have been calibrated[2] against a standard flow measuring device and for this the actual intakes were replaced by bellmouths with 4:1 contraction ratio.

Test details

All tests were made in the Royal Aircraft Establishment 3ft × 3ft wind tunnel at values of Reynolds number within the following ranges:

M_∞	Subsonic	1.41	1.71	2.00
$Re/10^6$	0.52-0.78	0.36-0.46	0.28-0.39	0.21-0.29

These values of Reynolds number are based on intake height h_e for rectangular intakes and radius r_e for semi-circular intakes.

Rectangular intakes with rounded corners, Fig.2(a) and with square corners, Fig.2(d) and semi-circular intakes, Fig.2(e), have been tested and in the discussion which follows results are selected specifically to illustrate particular drag components and do not necessarily form a complete set of data that is consistent in terms of intake configuration. Intake geometries are not defined in detail but the main features of each particular configuration used are included with the results. All tests were made at zero incidence of the fuselage datum. The rectangular intakes with rounded corners were aligned with the fuselage datum and all other intakes were canted down at $2\frac{1}{2}^\circ$ relative to this.

Results of preliminary experiments, which were made to survey the fuselage flow in the plane of the intake are shown in Fig.4. Fuselage boundary layer profiles were measured over the span of the intake at both subsonic and supersonic speeds and Mach number distributions were measured at supersonic speeds. The mean local Mach numbers of the flow external to the boundary layer are:-

M_∞	1.41	1.71	2.00
M_L	1.46	1.75	2.01

In the present tests, transition of the boundary layers on the cowl and endwall external surfaces has not been fixed artificially. If the cowl external flow is attached (as might be expected under conditions of high internal flow), because of the small scale and fineness of the cowl lips and the low Reynolds number of the tests, transition will not necessarily occur at the cowl lip. Fixing transition in this vicinity by a roughness band would introduce an effective modification to both the lip thickness and initial cowl external profile and thus possibly alter the drag characteristics of the intake. If however, because of spillage of air from the intake, separation of the flow from the cowl external surface does occur, it might be expected that on reattachment the boundary layer would be turbulent and transition would be fixed in this way. Simple calculations indicate that the difference in total external drag between a case in which there is a fairly extensive region of laminar flow on the cowl external surface and one in which transition occurs at the cowl lip is of the order $\Delta C_{D_E} = 0.02$.

Discussion of results at subsonic speeds

Maximum intake mass flow

Experimental results are presented as curves showing the variation of total external drag with intake mass flow ratio. These curves are referred to as external drag curves.

At subsonic speeds the maximum internal flow which can be achieved is limited by choking of the flow in the intake throat. The drag of the model at this condition is defined as the full flow drag and any change from this value, which results from a change of internal flow, is defined as spillage drag. It was not possible to pass sufficient flow in all of the intake configurations to achieve choking in the intake throat. For those intakes in which it was possible, the measured values of flow agreed with calculation to within about 1%. In other cases, when the maximum internal flow which could be obtained was limited by duct exit size,

measured external drag results are extrapolated to the conditions calculated for choked flow.

Cowl external flow-rectangular intake

Details of the external surface flow patterns associated with spillage of air from the intake were recorded using the surface oil flow technique. As an example, photographs of flow patterns obtained at M_∞ = 0.60 corresponding to various conditions on the external drag curves are shown in Fig.5. At low spillage, photographs 1 and 2 indicate a small bubble separation at the lip with attached streamwise flow over the remainder of the cowl surface. As spillage increases the size of the separation increases (photograph 3) until most of the cowl is in a region of separated flow (photograph 4). A schematic interpretation* of the cowl surface flow pattern corresponding typically to photographs 5 and 6 is shown in Fig.6.

Effect of swept endwalls - rectangular intake

Fig.5 also illustrates the effect on drag of changing from an unswept to a swept endwall shape. Swept endwalls give a lower value of drag at full flow but a considerably steeper rise in drag as flow is reduced.

Swept endwalls have a larger wetted area and thus some (small) increase in skin friction drag would be expected. However, in this particular design, they have the effect of fairing the steep external profile of the unswept endwall configuration, (c.f. Figs.2(d) and 2(f)) and consequently of altering the local fineness ratio. It is not clear whether this or the fact that swept endwalls prevent lateral flow, is the reason for the lower measured drag at full flow. Under spilling conditions prevention of lateral flow by swept endwalls means that, to a large extent, spillage is confined to the cowl. At points 4 and 5 on Fig.5, the two configurations produce similar values of external drag for a difference in internal flow of about $\Delta A_\infty/A_h = 0.13$. Corresponding cowl surface flow patterns indicate a similar size of flow separation in the two cases and thus similar values of flow spilled over the cowl and cowl drag might be expected. If this is so, the difference noted in internal flow is achieved by sideways spillage over the unswept endwalls for no penalty in drag. This might be expected because firstly, the endwalls are operating at relatively low spillage and secondly, their external profile has a high slope.

Effect on drag of varying compression surface geometry

External drag curves for rectangular and semi-circular intakes with sharp lipped cowls are shown in Figs.7 and 8 respectively. In each case results for various configurations of compression surface are included and these show that the external drag at full flow is virtually invariant with compression surface geometry. Thus, as has been observed previously[4] substantial flow spillage may be achieved with little drag penalty provided that the compression surface is adjusted to keep the intake throat Mach number high. Constant drag is obtained as the full flow condition is approached for the rectangular intake at M_∞ = 0.70 and for the semi-circular intake at M_∞ = 0.70 and 0.90 (extrapolated results) and therefore, at these conditions, in order to achieve a minimum drag penalty as air is spilled, a Mach number greater than 0.7 to 0.8 would have to be maintained in the throat. At M_∞ = 0.90 for the rectangular intake (except for $\delta_2 = -10^\circ$), there is no such constant drag condition and thus for minimum drag, in this case, the throat Mach number would have to be maintained at close to unity.

Included on Fig.7 are curves (annotated as maximum cowl thrust) showing the variation of spillage drag with internal flow calculated on the assumption of no change in cowl thrust as internal flow is reduced. These curves show the total pre-entry drag, $C_{D\ PRE}$, calculated by analysis of the forces for a control volume bounded by the internal flow between a station at infinity upstream and the inlet station i (see Fig.3)[5] where:-

$$C_{D\ SPILL} = C_{D\ PRE} = (p_m - p_\infty)\frac{1}{q_\infty}\frac{A_R}{A_e} + \left[q_i + \frac{1}{2}(p_i - p_\infty)\right]\frac{2}{q_\infty}\frac{A_i}{A_e}\cos\theta_i - 2\frac{A_\infty}{A_e}$$

and it is assumed that $p_m = \dfrac{(p_i + p_\infty)}{2}$.

Effect on drag of the presence of a compression surface

Tests on both a semi-circular and a rectangular intake with rounded corners have indicated that the value of external drag at full flow is lower when the intakes are of pitot type than when there is a compression surface present. Typical measured external drag curves for these cases are shown in Fig.9.

The presence of a compression surface will introduce additional wetted area on its under surface (i.e. the side adjacent to the fuselage). Also, for both model configurations used in the illustration, additional wetted area arises as indicated on the sketches contained in Fig.9. An increment in skin friction drag, which will appear as external drag, would therefore be expected from the introduction of a compression surface but simple calculations (using flat plate skin friction data[1]) indicate that this increment will be very much smaller than that measured. Thus at present the drag increment caused by the presence of a compression surface is not explained but attention is drawn to it because the magnitude of the increment is significant and it is consistently measured at subsonic speeds in the wind tunnel.

* This interpretation is annotated in a manner similar to that used in Ref.3.

It is possible that any air spilled over the sharp edges of the compression surfaces, in the manner sketched in Fig.9, would cause separations in the external flow and the drag associated with these would appear as additional external drag. Some water tunnel observations[6] on a semi-circular intake with a half-cone compression surface have indicated this sort of flow pattern.

Effect of cowl lip radius and external profile

This has been measured for both rectangular and semi-circular intake configurations and external drag curves are shown in Fig.10. In each case three cowls were tested, in which the different lip radii were followed by initial external profiles that were similar (i.e. parallel to each other) to a point about 0.7 h_e downstream from the lip (Fig.10). Aft of this point, differences were introduced to allow the cowls to blend into the same maximum section.

Results for the rectangular intake indicate that at high internal flow, values of external drag for the sharp lipped cowl are higher than those for blunted lip cowls. As spillage is increased the difference becomes smaller and at spillages greater than $\Delta A_\infty/A_h = 0.15$ to 0.20 below full flow, drag is no longer sensitive to lip radius.

As discussed earlier, the cowl surface flow patterns at $M_\infty = 0.60$ in Fig.5 indicate a small bubble separation at the cowl lip at high internal flow. It is presumably the extent of this separation which determines the cowl drag, and thus the value of total external drag at full flow. The mass flow ratio at which flow separation at the cowl lip occurs will depend on both lip geometry and the incidence of the lip to the local flow direction which will, in turn, depend on the spill flow quantity and the compression surface geometry. Cowl flow conditions which could account for the measured changes in drag are sketched on Fig.10. Condition (c), at which the flow may be attached for both cowls is not intended as a true extrapolation of the measured results but is drawn to illustrate that little difference in drag would be expected at this condition.

Results included in Fig.10 for the semi-circular intake configuration indicate that there is little effect of cowl lip radius on either the drag at full flow or the spill drag. On the basis of the above discussion this would indicate that at the full flow condition for this configuration, cowl flow separation is present for each lip, corresponding to condition (a) noted for the rectangular intake.

External drag curves for two rectangular cowls with rounded corners which have similar lip radii but different subsequent external profiles are shown in Fig.11. These results illustrate that in this case the values of external drag at full flow are similar but the spill drag characteristics are different.

The evidence of the results illustrated above therefore indicates that the cowl drag at full flow is largely dependent upon the radius at the cowl lip whereas the spillage drag characteristic is more dependent on the subsequent external profile of the cowl.

Results at supersonic speeds

Full mass flow and changes in drag at this condition

Full mass flow and drag under conditions when compression surface and cowl lip shocks are attached affords an opportunity for comparisons to be made of measured values with theoretical values which, in this case, may be calculated with some precision by using the theoretical shock geometry for the intake in the local fuselage flow and then relating to free stream conditions. Some examples of measured and calculated values of full flow are shown in Fig.12 for both semi-circular and rectangular intakes with a range of compression surface geometry. For the semi-circular configuration, Fig.12(a), agreement is generally good except for the pitot intake ($\theta_\ell = 90^\circ$) at $M_\infty = 2.00$, where measured results are 2% to 3% higher than the calculated values. This could be due to the influence on the external boundary layer of the intake shock wave which may be detached from the lip of the diverter passage as indicated in the sketch on Fig.12(a). For the rectangular intake, Fig.12(b), the calculated values of full flow do not allow for the effects of spillage of air over the swept endwalls. This is presumably the reason for the difference between measurement and calculation of 3% to 5% when all shocks are (theoretically) attached. When the endwall configuration is changed from swept to unswept, a further spillage occurs amounting to about 3% at $M_\infty = 1.41$ and 5% to 7% at $M_\infty = 2.00$, again when all shocks are attached. When the cowl lip shock is detached, for example at $M_\infty = 2.00$, $\delta_2 = 11.5^\circ$ the measured values of full flow for both endwall configurations are almost identical. This may be because the effect of removing swept endwalls is to reaccelerate the flow behind the oblique shock (by allowing lateral expansion), which possibly allows reattachment of the cowl lip shock. Hence, increased spillage over the unswept endwalls may be balanced by the elimination of spillage over the cowl. Included in Fig.12(b) at $M_\infty = 2.00$, are results obtained from measurements[7] with a model designed specifically for investigation into internal efficiency. Excellent agreement with the results of the present tests is noted.

Differences in drag at full flow between the semi-circular intake with and without the half-cone compression surface are plotted as a function of lip position angle θ_ℓ in Fig.13(a). The increase in drag as the cone shock moves forward of the cowl lip is in good agreement with the variation of pre-entry drag[8], calculated by integration of the pressures acting on the boundary of the entering stream tube between the cone shock and the intake. However there does appear to be a constant increment, particularly at $M_\infty = 2.00$, not allowed for in the calculation which could be due to the effect of the cone shock pressure rise on

the wedge diverter. The measured increment for a sharp lipped configuration (ΔC_D = 0.02 to 0.04) is about one-third of that which would be calculated on the simple basis of pressure rise times diverter projected frontal area.

As no rectangular pitot version of this intake was tested, changes in drag shown in Fig.13(b) are referred to the value for the configuration in which $\delta_2 = 0^\circ$ (i.e. a single 10° wedge). For the configuration with swept endwalls at M_∞ = 2.00, drag increments measured for $\delta_2 = 4.75^\circ$ and 11.5° are greater than the changes in pre-entry drag predicted by calculation. This discrepancy might be expected, since measured mass flows are lower than those predicted for these cases.

Changing endwalls from swept to unswept does not alter the total cowl projected area but, as discussed earlier, does alter the endwall external profile considerably (c.f. Figs.2(d) and 2(f)); for instance, in the region close to the fuselage the initial slope of the cowl changes from about 11° to 30°. A rough calculation of the change in cowl wave drag[9] for this change of profile at M_∞ = 2.00 gives $\Delta C_D = 0.087$. This is reasonably close to the measured change $\Delta C_D = 0.075$. This measured increment will contain the drag associated with the additional spillage over the unswept endwalls. Assuming this is similar to that calculated for twodimensional forespillage[10] the drag, for say 5% spillage, would be about 0.012.

Spillage drag

Drag coefficient is plotted as a function of intake mass flow for the semi-circular pitot intake in Fig.14. Measured values of spillage drag (i.e. increments relative to the values of drag at full flow) are shown and may be compared with two curves obtained by calculation. The first shows the spillage drag calculated[11] simply by multiplying the spillage area ($A_h - A_\infty$) by the pressure rise across a normal shock, and the second shows the pre-entry drag obtained by calculation of the change of momentum in the internal flow between free stream and the inlet. Comparing slopes of the measured and calculated curves (i.e. the rate of drag rise with spillage) reasonable agreement is achieved at M_∞ = 1.71 (Fig.14(b)) but not at the other Mach numbers. In general the method of calculating spillage drag[11] is known to give an overestimate at low supersonic Mach numbers (e.g. M_∞ = 1.41) where it underestimates the favourable changes in cowl drag with spillage. In Fig.15 changes in cowl drag, ΔC_{D_C}, i.e.

$$C_{D\ PRE}\ \text{(calculated)} - C_{D\ SPILL}\ \text{(measured)}\ ,$$

at M_∞ = 1.41 are plotted as a function of flow spillage and the present results are compared with those[12] for an isolated axi-symmetric pitot intake at M_∞ = 1.42. The changes in cowl drag with spillage are rather larger for the present semi-circular intake and this could be due to the higher initial slopes of the cowl and to the presence of a boundary layer diverter whose pressures might be affected favourably by subsonic forespillage. At M_∞ = 2.00 (Fig.14(c)) the slope of the measured spill drag curve is considerably lower than that of either of the two calculated curves. This is in contrast to results included in Fig.15 for the isolated axi-symmetric intake at M_∞ = 1.86, which show a smaller decrease in cowl drag with increasing spillage as Mach number increases and thus a better agreement with the simple method of spillage drag calculation might have been expected. A possible explanation of the lower measured slope may be the interaction between the intake shock and fuselage boundary layer which provides a branched shock configuration typically as sketched in Fig.14(c). A calculation may be made of the pre-entry drag associated with supersonic forespillage around a wedge[10] by assuming the separation resulting from the interaction as being equivalent to a 12° wedge (approximately the angle of the separated flow region). A curve of spillage drag calculated in this way is included on Fig.14(c) and the slope of the measured curve compares more favourably with this than with that calculated assuming subsonic forespillage behind a normal shock. When a half-cone compression surface is introduced into the semi-circular intake, spillage drag has been predicted by the methods of Ref.13. In this reference drag is calculated from the external shock pattern which is itself obtained from consideration of the balance between internal and spilled flow. In many cases this calculation results in a curve which has a discontinuity in slope. The change in slope occurs when the vortex sheet from the intersection of the conical shock and the detached normal shock crosses the cowl lip. The mass flow at which this happens will be the condition at which shock oscillation ('buzz') will occur according to the Ferri criterion[14]. Results are plotted in Fig.16 and there is fair agreement between both measured and predicted slopes of the spillage drag curves and the occurence of buzz for the lip angle position $\theta_\ell = 40^\circ$ at M_∞ = 1.71 (Fig.16(c)) and 2.00 (Fig.16(a)) but not good agreement at M_∞ = 1.71 with $\theta_\ell = 45^\circ$ (Fig.16(d)). When θ_ℓ is greater than the cone shock angle θ_w, the intersection point between the cone shock and the detached shock in front of the cowl lip is always within the intake bounding streamline and in this case, spillage drag is predicted exactly as for the pitot intake. This condition exists at M_∞ = 2.00 with $\theta_\ell = 45^\circ$ ($\theta_w = 42.5^\circ$) and Fig.16(b) shows good agreement between the slopes of measured and calculated spill drag curves. This is in contrast to results for the pitot intake, discussed above and illustrated in Fig.14(c) and it is evident that, in this case, the interaction of the intake terminal shock with the external boundary layer does not seriously modify the flow pattern. This is either because of the lower Mach number of the

terminal shock or because the interaction is inhibited by the presence of a compression surface.

Changes of drag at full flow with increase in cowl lip radius for the semi-circular pitot intake are shown in Fig.17(a). At $M_\infty = 1.41$ drag increases with increasing bluntness of the lip, at $M_\infty = 2.00$ it decreases. In addition to force measurements, at $M_\infty = 2.00$ increments in drag due to lip bluntness have been calculated from analysis of the bow shock shape[15] measured from schlieren photographs. These drag increments are shown in Fig.17(b) and are seen to compare well with force measurements. A comparison has also been made when the intake (with $r_\ell/r_e = 0.022$) is spilling 6% of the internal flow and again agreement between the two methods of measurement is very good.

When a compression surface is added to this intake the increment in drag (force measurements only) increases with increasing cowl lip radius at all Mach numbers, Figs.17(c) and 17(d). This trend has also been recorded for isolated axi-symmetric intakes with[16] and without[17] a conical compression surface. It is difficult from this evidence to decide whether the difference in behaviour between the present intake with and without a compression surface is intrinsic or whether it is due to changes in interference effects associated with the proximity of the intake to the fuselage boundary layer and to the wedge diverter.

Diverter drag

To evaluate the drag associated with a wedge shaped diverter for the fuselage boundary layer, tests were made on a rectangular intake with rounded corners with three values of diverter depth, h_D (see Fig.3). These values are given by $h_D/h_e = 0$, 0.111 and 0.190 and are shown drawn to scale relative to the fuselage boundary layer in Fig.4.

When $h_D/h_e = 0$ the compression surface leading edge is in contact with the flat fuselage side and the drag associated with the area of fuselage upstream of this, which is wetted by the internal flow, area A, Fig.18, is measured as part of the internal drag. The skin friction drag associated with this area may be calculated[1] and the drag values measured with $h_D/h_e = 0$ corrected accordingly.

When $h_D/h_e > 0$ three areas D, F_F and F_I (Fig.18) are exposed on which additional drag is incurred and again the skin friction drag associated with these areas may be estimated[1]. Table 1 shows increments in drag, measured from a datum level at $h_D/h_e = 0$, due to changes in h_D and also the associated estimated changes in skin friction drag. The difference between the two gives an indication of the diverter pressure drag.

Fuselage and installed intake pressure drag

Methods are available by which the wave drag of bodies of revolution and ducted bodies in supersonic flow may be predicted. These methods usually apply to idealised configurations and it is of interest to know whether predictions using these data for practical fuselage shapes and installed intake configurations will be of sufficient accuracy to be of use in design. An attempt has been made to study this by using a combination of measured drag and estimated skin friction drag (calculated using flat plate skin friction data[1]) to arrive at a value of pressure drag which may then be compared with predicted value. This analysis has been done over the free stream Mach number range 0.60 to 2.00 and results are presented in Tables 2 to 4.

Data for the 'fuselage' and 'fuselage plus canopy' configurations are shown in Table 2. Using the notation indicated in the table the pressure drag coefficient C_{D_p} is given by:-

$$C_{D_p} = C_{D_E} - C_{D_f} .$$

When the flow is entirely subsonic the pressure drag is approximately zero. When the flow becomes critical, in the region of the fuselage shoulder and on the canopy, as indicated by the schlieren photographs included in Table 2, the values of pressure drag are of sufficient accuracy to show a drag increment.

At supersonic speeds comparison of estimated wave drag[9] and experimentally derived pressure drag for the fuselage is reasonably satisfactory at $M_\infty = 1.41$ and 1.71 but at $M_\infty = 2.00$, the pressure drag is rather high. Two methods are used to estimate the wave drag of the fuselage and canopy. In the first, method (a), the canopy is assumed to alter the fineness ratio of the body as a whole by effectively moving the position of the maximum cross section forward. The second, method (b), treats the canopy as a separate body in the local fuselage flow and its wave drag is calculated and added to that of the fuselage to give the wave drag of the combination. Method (b) gives results which are closest to the derived pressure drag and again in this case agreement is quite good at $M_\infty = 1.41$ and 1.71 but at $M_\infty = 2.00$ the pressure drag is high.

In Table 3 the drag analysis is given for the model with rectangular intakes with unswept endwalls, $r_\ell/h_e = 0.022$ and $\delta_2 = 0^\circ$. Using the notation indicated in this table the installed cowl pressure drag C_{D_C} (INST) is given by:-

$$C_{D_C}(\text{INST} = C_{D_E} - \left\{ C_{D_{(F+C)}} + C_{D_f}(\text{INST}) + C_{D_W}(\text{DIV}) + C_{D_{\text{PRE O}}} \right\}$$

CORRIGENDA

THE EXTERNAL DRAG AT SUBSONIC AND SUPERSONIC SPEEDS OF FUSELAGE-SIDE AIR INTAKES FOR STRIKE-FIGHTER AIRCRAFT

M D DOBSON and E L GOLDSMITH

PAGE 3 COLUMN 2

PARAGRAPH BEGINNING "Included on Fig 7".....

AFTER WORDS "ASSUMPTION OF" INSERT:-

..... "complete cancellation of pre-entry drag by thrust forces developed on the cowl. These are simply curves of constant drag drawn at the mean of the full flow drag levels of the measured results. Also included are curves (annotated as "zero cowl thrust") which show the variation of spillage drag calculated on the assumption of ....."

Fig 17

SCALE OF r_c/r_1 SHOULD READ 0.01, 0.02, 0.03 etc.

where C_{D_f} (INST) is the nacelle installation skin friction drag coefficient, which referring to Fig.18, is the sum of the skin friction drags of:-

$$\text{area E} + \text{area F}_I + \text{area D} - \text{area B} .$$

C_{D_W} (DIV) is the diverter pressure drag coefficient related to this installation using the values of C_{D_D} given in Table 1, and

$C_{D_{PRE\ 0}}$ is the calculated pre-entry drag at the condition of maximum measured mass flow, assuming that the intake terminal shock is attached to the lip and thus all flow is spilled supersonically. A similar drag analysis is given in Table 4 for the model with semi-circular sharp lipped pitot intakes. For both of the above configurations cowl wave drag has been estimated from Ref.9, which uses a combination of slender body and quasi-cylinder theories and assumes the internal flow to have no influence on wave drag. For both of these configurations the experimentally derived pressure drag coefficients are similar and increase with increasing supersonic free stream Mach number, whereas the estimated wave drag coefficients do not. In the worst case, at $M_\infty = 1.41$ for the rectangular intake, the difference between the two values is just less than 14% of the measured total external drag.

At subsonic speeds this analysis gives a cowl pressure drag coefficient of approximately zero for the rectangular intake configuration but about 0.045 for the semi-circular configuration. The reason for this difference is not understood. The installation skin friction drag is similar in the two cases but the measured drag is higher for the semi-circular intake configuration. Both intake designs have approximately the same capture area and both blend into similar maximum sections at approximately the same distance downstream from the lip. However local cowl external profiles are different, particularly in the regions close to the fuselage (c.f. Figs.2(d) and 2(e)).

Concluding remarks

An experiment is described from which measure-measurements of the drag associated with fuselage side intake installations are obtained at both subsonic and supersonic speeds. The experiment is shown to provide versatility in the range of intake configurations which may be tested and the accuracy of measurement is shown to be adequate for the determination of components of external drag resulting from relatively small variations in intake and installation geometry.

Drag at full flow as well as drag due to spillage has been measured, and for a rectangular intake, cowl external surface flow patterns under conditions of intake spillage have been observed. The effect of changing endwall geometry of a rectangular intake has also been examined and the effects of cowl lip radius, cowl external profile and compression surface geometry have been investigated for both rectangular and semi-circular types of intake.

Using the experimental data the wave drag of a wedge shaped diverter for the fuselage boundary layer has been derived at supersonic speeds and the wave drag of installed intakes has been derived in a similar way. Results for the latter are shown to compare reasonably well with some estimates.

Symbols

A	area
C_D	drag coefficient
D	drag
h	height
M	Mach number
p	static pressure
q	dynamic pressure
r	radius
R_e	Reynolds number
γ	ratio of specific heats
δ_2	compression surface angle (see Fig.3)
θ	angle
Δ	increment

Suffixes

BAL	balance
BASE	model base
C	cowl
D	diverter
e	'entry' (defined in Fig.3(c))
E	external
f	skin friction
(F+C)	fuselage plus canopy
h	'highlight' (defined in Fig.3(c))
i	'inlet' (defined in Fig.3(b))
I	internal
ℓ	'lip' (defined in Fig.3(c))
L	local flow conditions external to the fuselage boundary layer
P	pressure
PRE	pre-entry
PRE 0	pre-entry at full internal flow
R	'ramp' (defined in Fig.3(b))
SPILL	spillage
W	wave
x	duct internal measuring station
∞	free stream station

References

1. Smith, K.G: Methods and charts for estimating skin friction drag in wind tunnel tests with zero heat transfer. ARC CP824., 1964.

2. McGregor, I: The characteristics and calibration of two types of airflow metering device for investigating the performance of model air intakes. RAE Tech Report to be published.

3. Green, J.E: Interactions between shock waves and turbulent boundary layers. RAE Tech Report 69098, May 1969.

4. Mount, J.S: Additive drag on inlet cowls and its effect on aircraft performance. AGARDograph 103, October 1965.

5. Neale, M.C: The drag of variable ramp intakes at high subsonic Mach number. NGTE Note Nt 653, May 1967.

6. Davenport, C: A further investigation of the drag at subsonic speeds of side intake boundary layer diverters. British Aircraft Corporation Report AX 316.

7. Brown, C.S., Goldsmith, E.L: RAE unpublished data.

8. Fraenkel, L.E: Some curves for use in the calculations of the performance of conical centre-body intakes at supersonic speeds at full mass flow. RAE Tech Note Aero 2135, December 1951.

9. Fraenkel, L.E: Curves for estimating the wave drag of some bodies of revolution based on exact and approximate theories. RAE Tech Note Aero 2184, August 1952.

10. Dutton, R.A., Goldsmith, E.L: The drag of some wedge centrebody intakes at Mach numbers of 1.56, 1.86 and 2.14. RAE Tech Report 66208, September 1966.

11. Seddon, J: Note on the spillage drag of pitot-type air intakes at transonic speeds. RAE Tech Note Aero 2315, August 1954.

12. Griggs, C.F., Goldsmith, E.L: Measurement of spillage drag on a pitot type intake at supersonic speeds. RAE Tech Note Aero 2256, August 1953.

13. Goldsmith, E.L., Griggs, C.F: The estimation of shock pressure recovery and external drag of conical centrebody intakes at supersonic speeds. R & M 3035, 1959.

14. Ferri, A., Nucci, L: The origin of aero-dynamic instability of supersonic inlets at sub-critical conditions. NACA RM L50 K36.

15. Pugh, P.G., Ward, L.C: The estimation of zero incidence forebody pressure drag coefficients of axi-symmetric bodies from measured bow shock shapes. NPL Aero Report 1245, August 1967.

16. Goldsmith, E.L., Griggs, C.F: A comparison of the estimated and measured performance of conical centrebody intakes at Mach numbers from 2.14 to 3.27. RAE Tech Note Aero 2276, November 1953.

17. Fraenkel, L.E: The external drag of some pitot type intakes at supersonic speeds, Part II. RAE Report Aero 2422, June 1951.

Table 1

DIVERTER DRAG COEFFICIENTS

	b_D/h_s	M_∞				
		0.60	0.85	1.41	1.71	2.00
Datum drag	0	0	0	0	0	0
Skin friction drag[†], area A correction	-	0.023	0.022	0.022	0.022	0.021
Skin friction drag increment	0 to 0.111	0.033	0.032	0.032	0.031	0.031
Skin friction drag total increment	0 to 0.111	0.056	0.054	0.054	0.053	0.052
Measured drag increment	0 to 0.111	0.047	0.046	0.072	0.069[*]	-
Skin friction drag increment	0.111 to 0.190	0.009	0.009	0.009	0.009	0.009
Skin friction drag total increment	0 to 0.190	0.065	0.063	0.063	0.062	0.061
Measured drag increment	0 to 0.190	0.059	0.056	0.113	0.116	0.097
Pressure drag of diverter	0.190	≃ 0	≃ 0	0.050	0.054	0.036
Diverter pressure drag coefficient based on diverter frontal area (C_{D_D})		≃ 0	≃ 0	0.084	0.090	0.060

† All skin friction drag increments have been calculated using flat plate data[(1)]. Some reservation must therefore be placed on the accuracy of increments calculated because, for example, area A, Fig.18, is nearly conical.

* In these cases some of the external boundary layer is ingested by the intake but no correction has been made for the consequent small part of external drag which has been included in the internal drag measurements.

Table 2

DRAG ANALYSIS - MODEL WITHOUT INTAKES

M_∞	0.60	0.70	0.80	0.90	1.41	1.71	2.00
	Drag coefficients						
Fuselage							
Measured drag (C_{D_E})	0.137	0.140	0.143	0.163	0.266	0.253	0.291
Calculated skin friction drag (C_{D_f})	0.140	0.144	0.144	0.157	0.164	0.161	0.156
Pressure drag (C_{D_P})	≃0	≃0	≃0	0.006	0.096	0.091	0.135
Estimated wave drag					0.114	0.110	0.103
Fuselage + canopy							
Measured drag	0.151	0.151	0.160	0.191	0.442	0.416	0.454
Calculated skin friction drag	0.142	0.146	0.146	0.159	0.166	0.164	0.158
Pressure drag	0.008	0.005	0.014	0.032	0.276	0.252	0.296
Estimated wave drag (method (a))					0.219	0.199	0.182
Estimated wave drag (method (b))					0.271	0.244	0.231

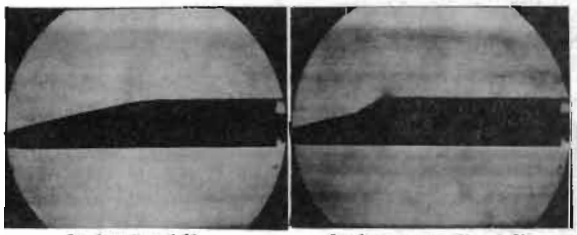

Fuselage M_∞ = 0.90 Fuselage + canopy M_∞ = 0.70

Table 3

DRAG ANALYSIS - MODEL WITH RECTANGULAR INTAKES

M_∞	0.60	0.70	0.80	0.90	1.41	1.71	2.00
	Drag coefficients						
Fuselage + canopy drag ($C_{D_{(F+C)}}$)	0.151	0.151	0.160	0.191	0.442	0.416	0.454
Installation skin friction drag (C_{D_f}(INST))	0.093	0.092	0.088	0.085	0.074	0.073	0.072
Divertar wave drag (C_{D_W}(DIV))					0.057	0.062	0.042
Pre-entry drag ($C_{D_{PRE\ 0}}$)					0.109	0.059	0.035
Total of above	0.244	0.243	0.248	0.276	0.682	0.610	0.603
Measured drag (C_{D_E})	0.239	0.250	0.251	0.286	0.785	0.820	0.830
Installed cowl pressure drag (C_{D_C}(INST))	≃0	≃0	≃0	0.010	0.103	0.210	0.227
Estimated cowl wave drag					0.211	0.171	0.151

Table 4

DRAG ANALYSIS - MODEL WITH SEMI-CIRCULAR PITOT INTAKE

M_∞	0.60	0.70	0.80	0.90	1.41	1.71	2.00
	Drag coefficients						
Fuselage + canopy drag	0.148	0.149	0.158	0.188	0.434	0.409	0.447
Installation skin friction drag	0.103	0.102	0.098	0.096	0.084	0.084	0.082
Diverter wave drag					0.056	0.061	0.041
Pre-entry drag					0	0	0
Total of above	0.251	0.251	0.256	0.284	0.574	0.554	0.570
Measured drag	0.295	0.299	0.300	0.329	0.720	0.770	0.795
Installed cowl pressure drag	0.044	0.048	0.044	0.045	0.146	0.216	0.225
Estimated cowl wave drag					0.207	0.167	0.148

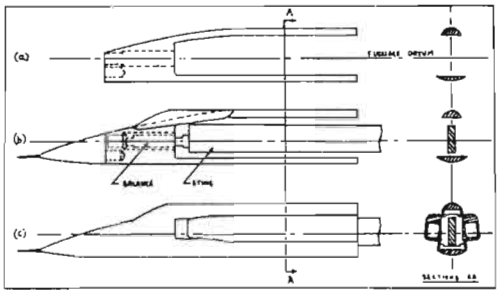

FIG1 SKETCH SHOWING MODEL ASSEMBLY.

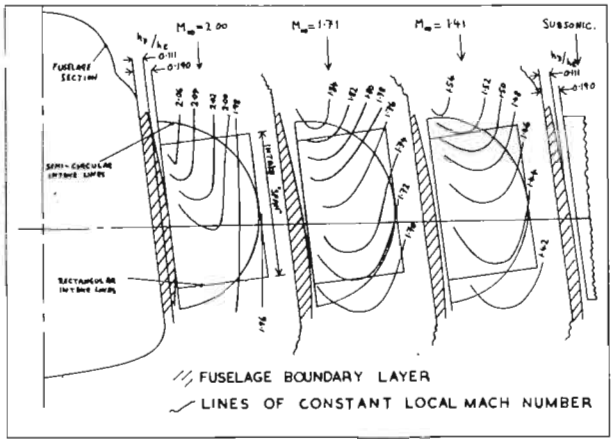

FIG 4 FUSELAGE FLOW FIELD CHARACTERISTICS

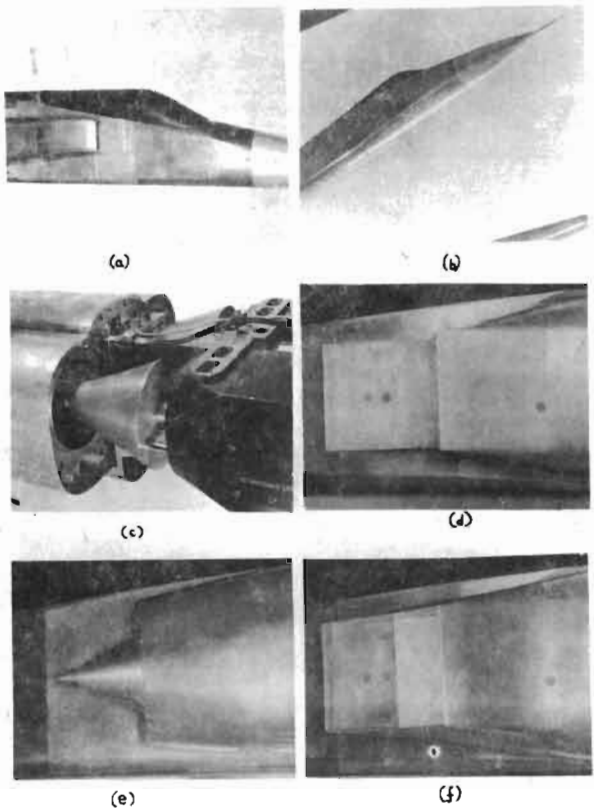

FIG 2 PHOTOGRAPHS OF MODELS

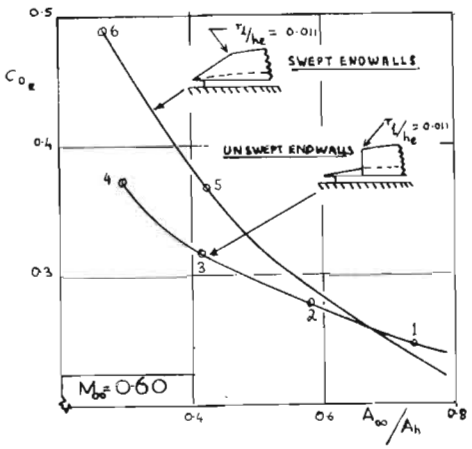

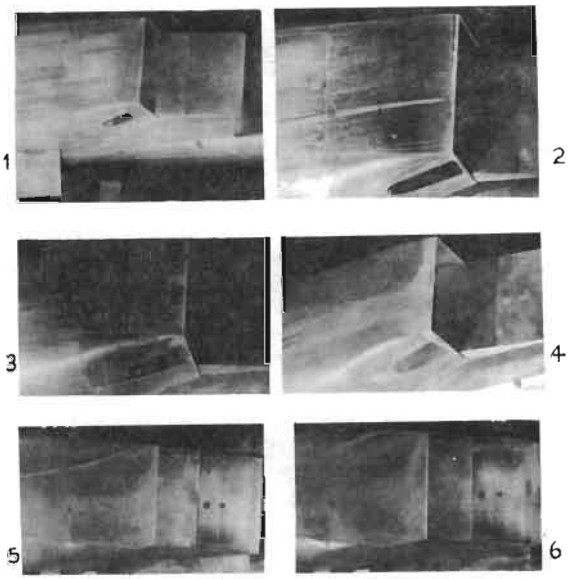

FIG 5 COWL EXTERNAL FLOW CHARACTERISTICS
RECTANGULAR INTAKE

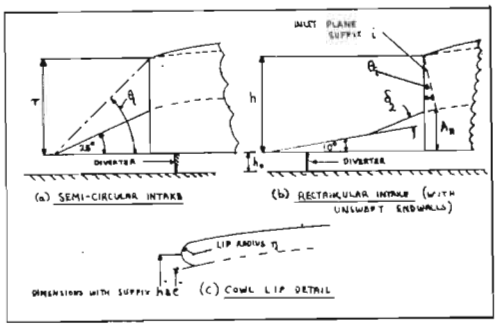

FIG3 DETAILS OF INTAKES

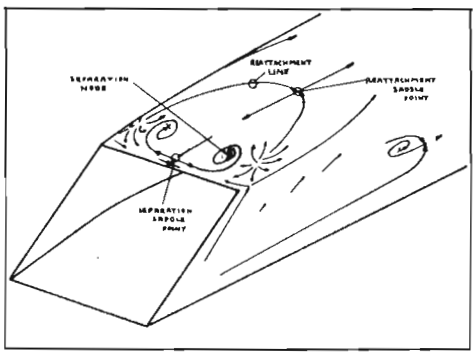

FIG 6. SCHEMATIC INTERPRETATION OF COWL SURFACE FLOW PATTERN

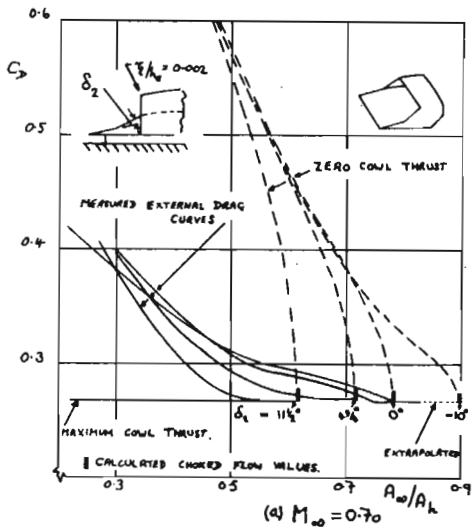

FIG 7 EFFECT OF COMPRESSION SURFACE GEOMETRY ON EXTERNAL DRAG — RECTANGULAR INTAKE

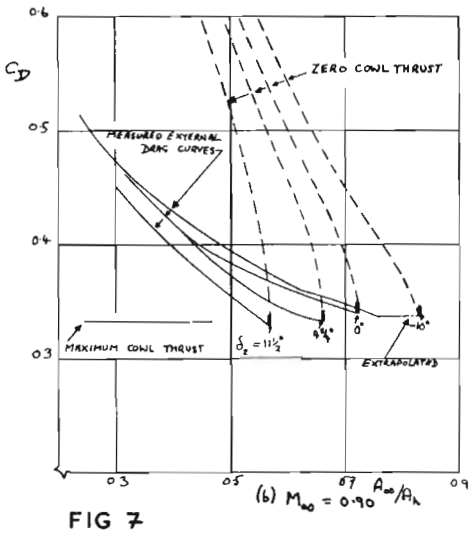

FIG 7

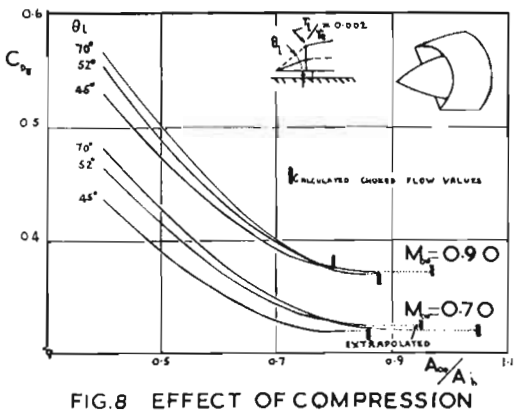

FIG.8 EFFECT OF COMPRESSION SURFACE POSITION ON EXTERNAL DRAG — SEMI-CIRCULAR INTAKE.

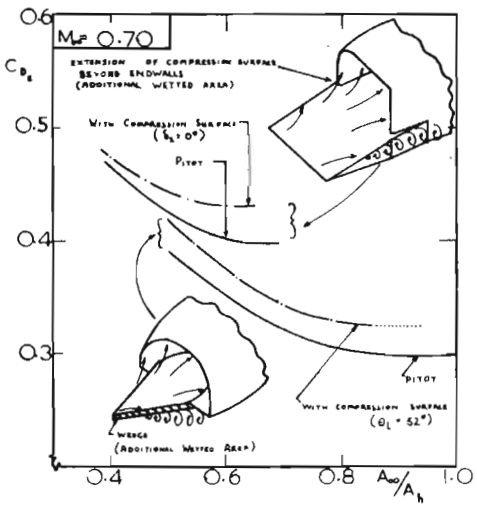

FIG 9 EFFECT OF A COMPRESSION SURFACE ON EXTERNAL DRAG

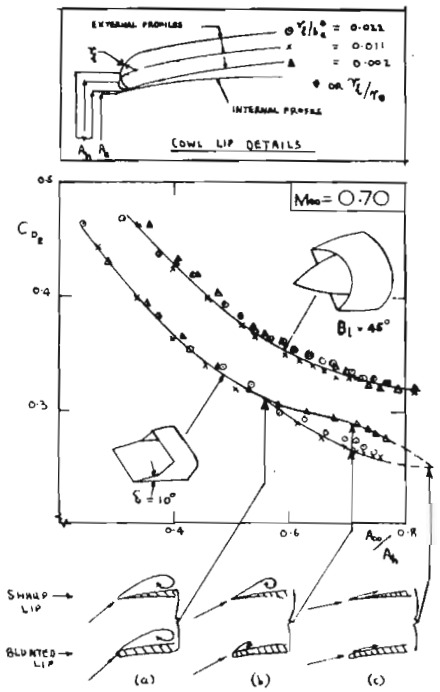

FIG 10. EFFECT OF COWL LIP RADIUS ON EXTERNAL DRAG

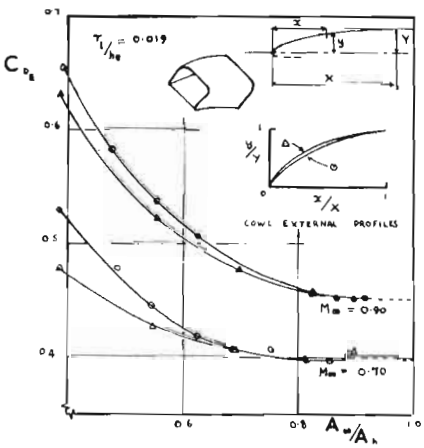

FIG 11 EFFECT OF COWL EXTERNAL PROFILE ON EXTERNAL DRAG

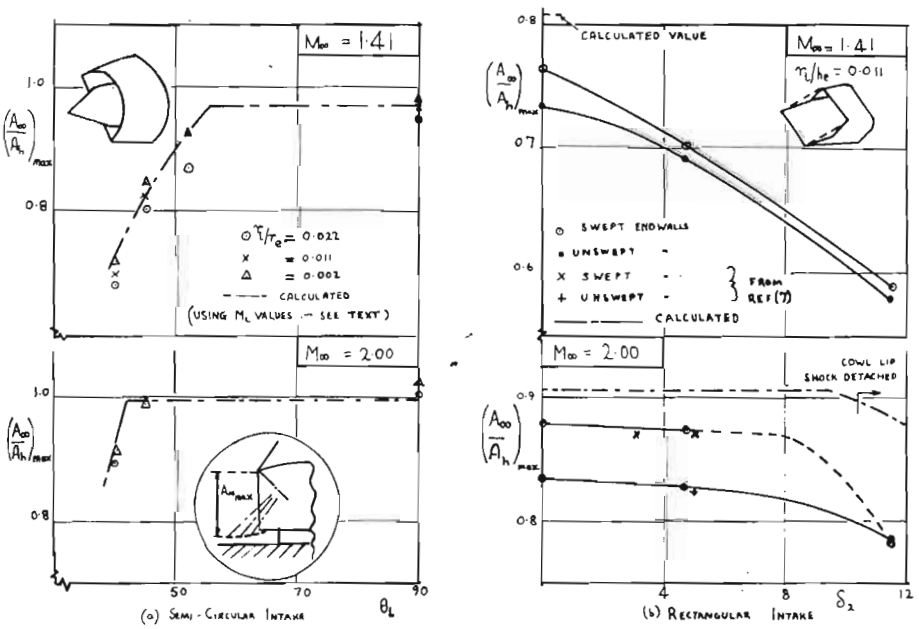

FIG 12 FULL MASS FLOW — COMPARISON OF MEASURED AND CALCULATED VALUES.

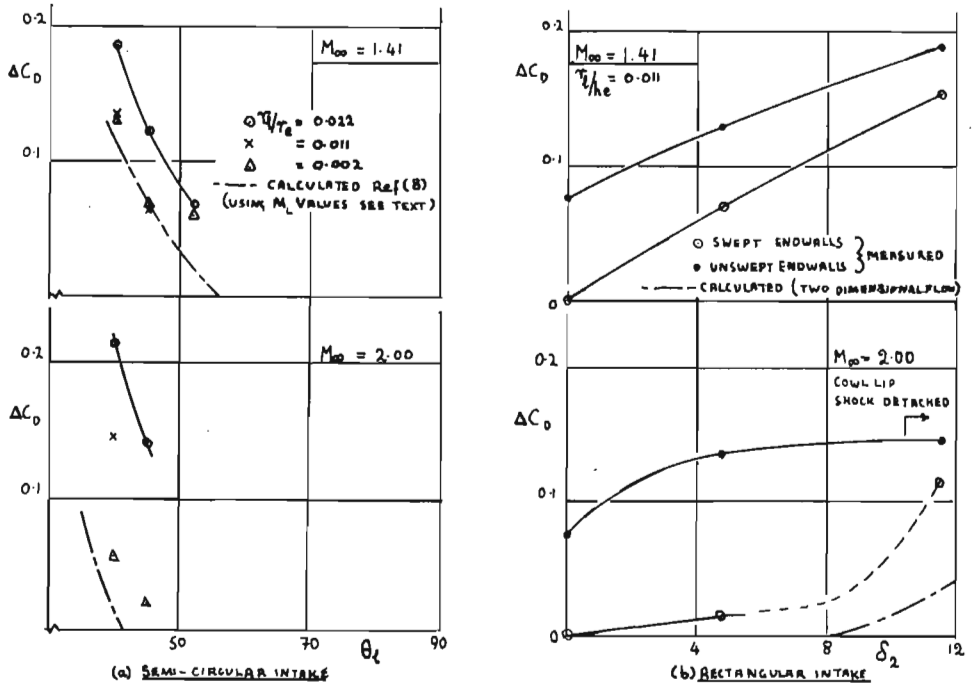

FIG. 13 DRAG AT FULL MASS FLOW — INCREMENTS DUE TO CHANGE IN INTAKE GEOMETRY.

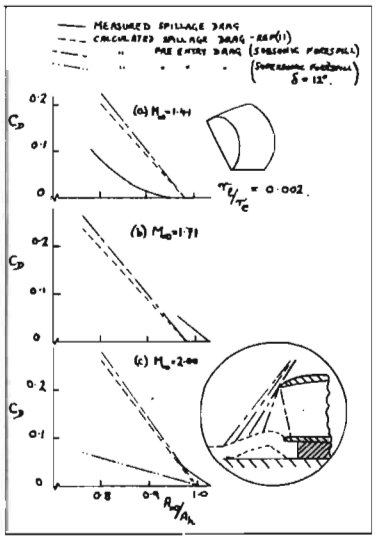

FIG 14. SPILLAGE DRAG — VARIATION WITH MASS FLOW RATIO FOR SEMI-CIRCULAR PITOT INTAKE

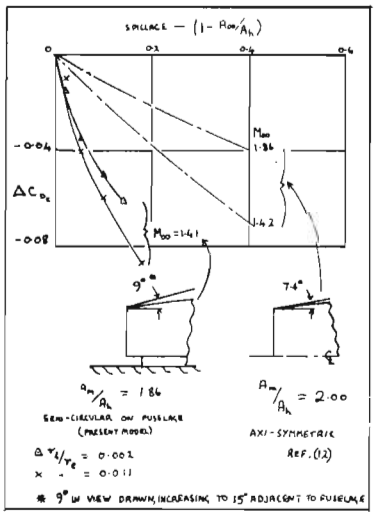

FIG 15. COWL DRAG — VARIATION WITH FLOW SPILLAGE

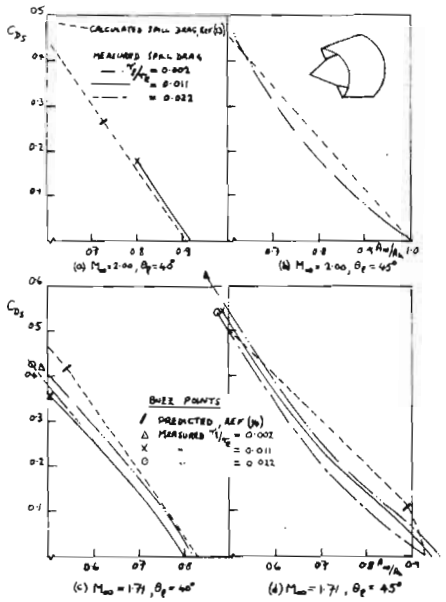

FIG 16 SPILLAGE DRAG – VARIATION WITH MASS FLOW RATIO FOR SEMI-CIRCULAR INTAKE WITH COMPRESSION SURFACE

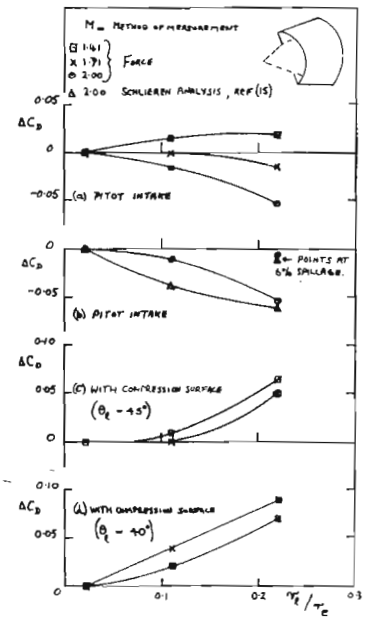

FIG 17. DRAG INCREMENT RESULTING FROM INCREASE OF COWL LIP RADIUS

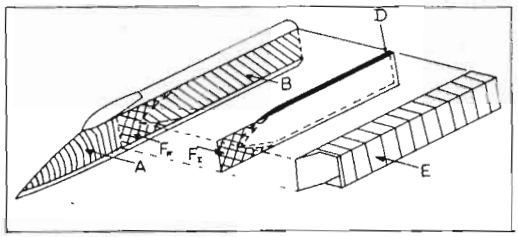

FIG 18 SURFACE AREAS FOR SKIN FRICTION ESTIMATION FOR DIVERTER & INSTALLATION DRAG ANALYSES